HPS calorimeter performances

HPS collaboration, Elsevier Inc[a,b], Global Customer Service[b,*]

[a]*1600 John F Kennedy Boulevard, Philadelphia*
[b]*360 Park Avenue South, New York*

Abstract

The Heavy Photon Search experiement (HPS) aims to discover a new particle called heavy photon, that is the equivalent of the photon of the Standard Model for dark matter. It is detectable through its mixing with the standard photon. HPS is installed in the Hall B of Jefferson Laboratory, Virginia, United States of America. After a test run in 2012 and an engineering run in 2014, a first run was performed to acquire data. This paper presents the performances of one of the two detectors of the experiment: the electromagnetic calorimeter (ECal).

Keywords: heavy photon, calorimeter, CLAS12, CLAS, Jefferson Laboratory, JLab

2010 MSC: 00-01, 99-00

1. Introduction

The heavy photon, also known as A' or dark photon, is a gauge boson that could be the equivalent of the ordinary matter photon for dark matter by being its electromagnetic force carrier. Heavy photons have been envisionned by numerous beyond Standard Model theories [**?**]. It is also a good candidate to explain some astrophysical anomalies [**?**]. The dark photon, that would interact with particles of the hidden sector, would mix with the ordinary photon through kinetic mixing [] (add ref). It induces their weak coupling to electrons, ϵe, they

---

*Corresponding author
Email address: support@elsevier.com (Global Customer Service)
URL: www.elsevier.com (Elsevier Inc)

can thus be radiated in electron scattering and consequently decay into electron-positron pairs. If the coupling is large enough, the resonance can be observed above the QED trident background, while if it is small enough, heavy photons travel detectable distances before decaying. The HPS experiment is designed to exploit both signatures. It will benefit of the full duty cycle of the electron beam available at JLab in Hall B to cover two areas depending on the heavy photon mass and the strength of its coupling. To cover the largest area possible, three runs are planned with the following beam energy: 1.1 GeV, 2.2 GeV and 6.6 GeV and a luminosity comprised between 200 nA and 500 nA. The silicon microstrip vertex tracker and the $PbWO_4$ electromagnetic calorimeter placed as close as possible of the 0.15% - 0.25% X0 tungstene target will then allow the HPS experiment to be sensitive to heavy photons in the mass range of 20 MeV/c^2 to 1000 MeV/c^2 (see fig. 1).
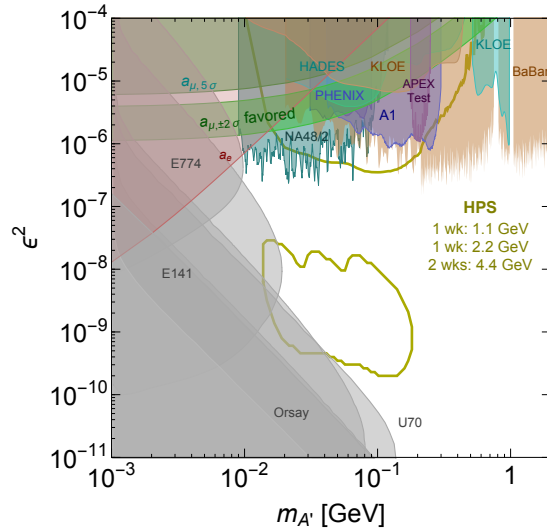

Figure 1: Coupling factor as a function of the mass of the heavy photon. In light green the area covered by the HPS experiment.

The experiment is installed in the Hall-B at Jefferson Lab. In addition to the detectors, an analyzing magnet allows to determine the charge and momentum

of the particles. Two magnets installed downstream and upstream of the target

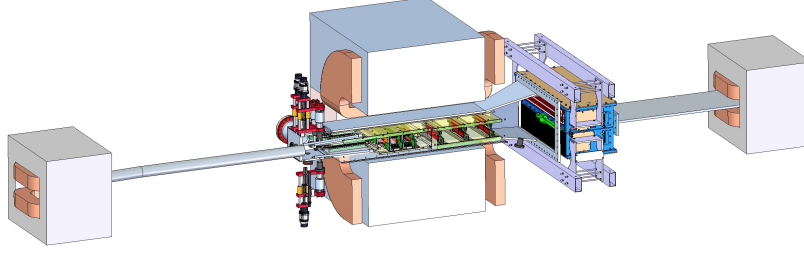²⁵ complet the setup to ensure that the beam reaches the beam dump (see fig. 2).

Figure 2: Schematic layout of the HPS experiment.

A test run was performed in May 2012 with a partial detector setup, which results can be found in [**?**]. We detail here the performances of the final calorimeter during the engineering runs of Winter 2014 and spring 2015. The paper is organised as follow: we first presents the calorimeter layout as well as

³⁰ the modifications made to the calorimeter after the test run. The two following sections are about the time and energy calibration of the detector. Eventually, a presentation of the performance of the LED system used to monitor the crystals is given.

(should we describe/discuss trigger? fADC? TDC? and pre-amplifiers?)

³⁵ **2. Calorimeter layout**

The ECal is built in two separate halves that are mirror reflections of one another about the plane of the nominal electron beam to avoid interfering with a horizontal 15 mrad zone of very high flux. This zone is due to the dipole magnet that spreads the degraded beam on a plane. As shown in Figure 4, the

⁴⁰ 221 modules in each half, supported by aluminum support frames, are arranged

3

in rectangular formation with five layers and 46 crystals/layer except for the layer closest to the beam where nine modules were removed to allow a larger opening for the outgoing electron and photon beams.

Each crystal (see fig. 3) is a 160 mm long tapered parallepiped with a front (rear) face of 13.3×13.3 mm^2 (16×16 mm^2). The crystals were previously used for the inner calorimeter of CLAS, they have been equipped with 10×10 mm^2 Large Area APD (LAAPD-Hamamatsu XXX) (**add product ref**). The new LAAPD allows to collect more light, those increasing the signal over noise ratio leading to a lower energy threshold and an improved energy resolution. The signal from the APDs is first sent to a preamplifier converting current-to-voltage (0.62 V/pC) which was designed to have low impedance and low noise (**add diagram and maybe more details or ref?**). Finally, 2/3 of the signal is sent to the fADC(**ref?**), the other part being sent to a TDC.

The gain of the APDs was chosen to be the best compromise between high gain and low dark current (**Do we have values/figures to motivate the choice then?**). The voltage of each APD group is then selected so that the gain is near 150 for each APD. (**add the equation and values to get MeV to V conversion**) The gain of the preamplifier was adjusted to 0.62 V/pC to ensure that maximum energy deposition, estimated to be 4 GeV in a single crystal, would not saturate the fADC.

In front of the crystals are installed LED placed in plastic holders to send iin the crystal either blue or red light. Their principaly used to check the functionning of the crystal and the amplification chain. In the future studies will be carried to study how they can help crystals to recover from radiation dammage.

To stabilize the crystal light yield and the operation of the APDs, each half of the calorimeter is enclosed in a temperature controlled box ($<1°$C stability and $<4°$C uniformity **Do we need a chart of Temp to illustrate?**). This is especially important because of the power drawn by the preamplifiers, 0.11 W each. The operating voltage of the preamplifiers (± 5 V), the bias voltage of the APDs (≈ 400 V), and the read out channels from the APDs are supplied
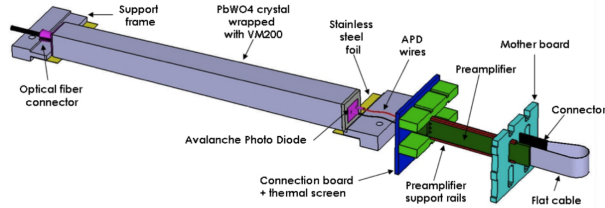
Figure 3: A schematic view of an ECal module.

by four new printed circuit boards mounted on the backplane penetrating the enclosure. They were completely redesigned after the 2012 test run and a very careful attention was brought to avoid cross-talks between channels. Each half of the ECal is divided into 14 bias voltage groups. Indeed, APDs are inherently produced with different gain to voltage characteristics. The cautious selection of APD groups, their matching with the preamplifiers and adjusting the high voltage lead to a total gain uniformity of about 2% (**confirmed by calibration data?**), which highly simplify our trigger setup.

During the run, both halves were held in place by vertical threaded rods attached to rails above the analyzing magnet. Surveys carried out before the runs have shown that the distance between the target and the front face of the crystals is on average XX cm. The gap between the two halves being XX cm, corresponding to a minimum incident angle of XX mrad. (**numbers to update**) The surveys have also shown that the initial positions of the two halves can be easily retrived within 0.3 mm after moving the detector out to access the SVT or do maintenance work.

2.1. LED monitoring system

Although relatively radiation tolerant, lead tungstate scintillating crystals do lower the light output when exposed to radiation and recover when the radiation source is removed, trough spontaneus thermal-annealing mechanisms. Extensive studies performed at the Institute for High Energy Physics (IHEP) in Protvino, Russia, confirmed that the $PbWO_4$ light output changes with the irradiation
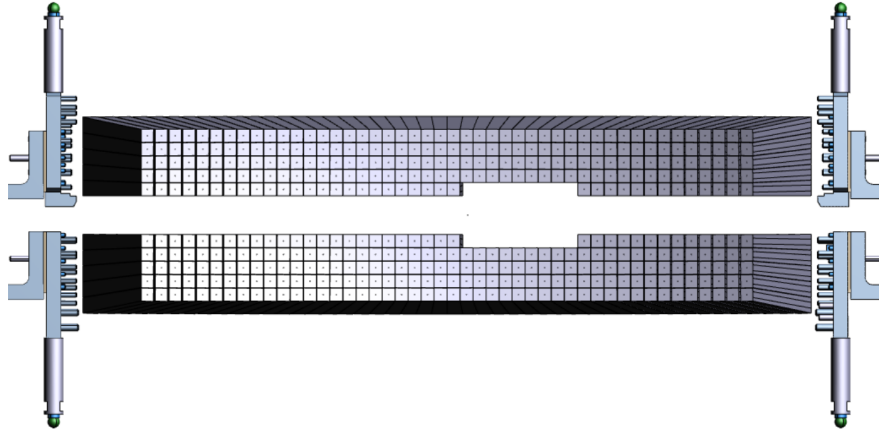
Figure 4: Schematic view of an ECal module.

dose rate. In particular, dedicated measurements showed that degradation of light output in $PbWO_4$ crystals occurs due to light transmission loss only, rather than changes in the intrinsic scintillation mechanism [?]. Further complications arise because at the same irradiation intensity, changes in light output may vary from one crystal to another [?] [?]. Add plot of radiation damage measurement here - and quote S.Fegan paper? Probably yes, since it also shows the effect of light annealing

In order to preserve the intrinsic ECal energy resolution, the response of the crystals has to be continuously monitored and, if necessary, recalibrated. To this end, a custom, LED-based monitoring system was specifically designed and installed in the detector setup after the 2012 test run. With this system, a light pulse, with variable amplitude and width, can be injected independently in each crystal. The pulse is emitted by a red/blue bi-color LED placed in front of the crystal. By measuring the response of the whole chain (crystal + APD + amplifier) to the pulse, any variation in the channel response can be acknowledged and, if necessary, corrected. Furthermore, since radiation damage in the $PbWO_4$ crystals is not uniform over the transmission spectrum, but is mostly concentrated in the blue region (up to $\simeq 500$ nm), the use of a red/blue bi-color LED can also help in determining which component in the chain is
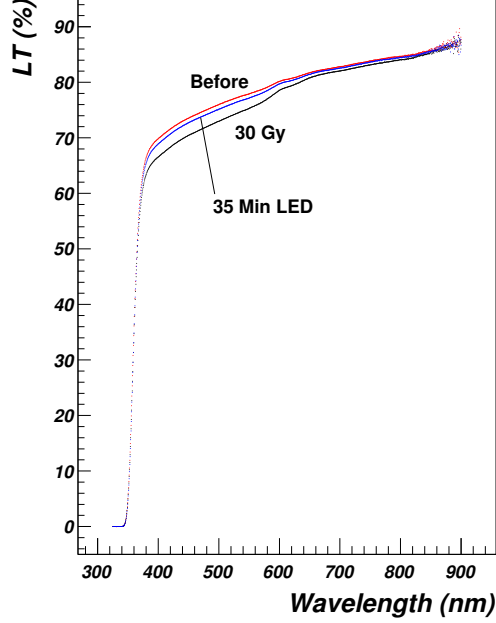
6

Figure 5: A schematic view of an ECal module.

responsible of a possible channel response variation. Given the possibility to turn on one or more channels at time, with a programmable pattern, such a system has been extensively used during the Ecal and trigger commissioning. Finally, studies are currently undergoing on the possibility to use the monitoring system to recover crystals radiation damage trough a light annealing mechanism. CITATION NEEDED

The LED monitoring system setup is as follows. Each LED is hosted in a PEEK plastic holder placed in front of the crystal, with a proper light collimation hole. LEDs are connected trough twisted-pair wires to 4 printed-circuit boards - two for Ecal top, two for Ecal bottom - that, in turns, are connected to 8 driver circuits, mounted directly on top and on bottom of the detector external enclosure. The drivers host the electronic circuits used to pilote the LEDs, and have them producing the light pulses, with programmable amplitude, width

and frequency. Drivers communicate with the main system controller via I^{2}C protocol. The controller, that also provides power and the master clock to the drivers, hosts a PIC32-based board, with a custom firmware, connected trough Ethernet to the HPS slow-controls network. More details?

3. Time calibration

The time calibration is a key element for our experiment as our trigger is based on the measurement coincidences in the two halves of the calorimeter. A good time precision reduces the occurance of accidental coincidences which we want to minimize. The time of a cluster is set from the crystal with the highest energy in this cluster. This signal, sampled at 250 MHz by a fADC, is fitted by the sum of a pedestal P and a $3 - pole$ function for the pulse with width τ and pulse time t_0 1:

$$P + \frac{A}{2\tau^2} \left(t - t_0\right)^2 e^{-(t-t_0)/\tau} \tag{1}$$

For each crystal the width of the $3-pole$ function is fixed to its average value to improve the time resolution [?]. An example of fit can be found Figure 6.
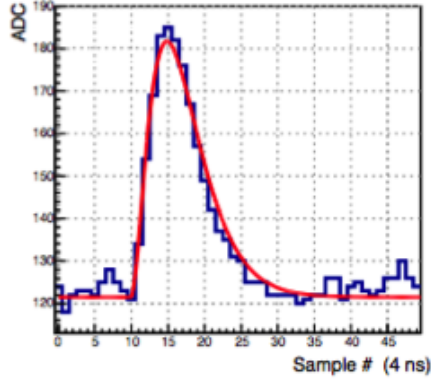

Figure 6: Example fit of an indivudual pulse. The resulting 3-pole function is drawn across the entire readout window for visualization, although the actual range fitted is smaller.

We show in this part how the time offsets for each channel are determined and how time walk and resolution vary as a function of the energy.

8

3.1. Offsets

The method used to obtained the time offsets T_{offset} implies to find the two paremeters of equation 2:

$$T_{offset} = 2.004 \cdot m + r \tag{2}$$

Where r is determined using the time difference between the radiofrequency (RF) signal and crystal signal. While m is obtained by using the time difference between two well-correlated clusters in an event.

The determination of r relies on the fact that the accelerator RF signal enters Hall B at 499 MHz and the accelerator provides a signal every 80 bunches that we measure on a channel of our fADC boards in the exact same conditions than our experimental signals. The precision at which the accelerator signal is measured has been determined to be 24 ps. This signal being sampled every 80 bunches the time difference between the RF signal and a crystal is expected to present peaks spaced by 2 ns as one can see Figure 7. At this step, it is not possible to determine the parameter m of eq 2 as the time difference between the RF signal and the event shows 2 ns steps. Nevertheless, by overlapping the peaks and centering them on zero, any offset lower than 2 ns can be found. This fine offset, r in eq 2, is obtained iteratively, usually two or three iterations are necessary to converge.
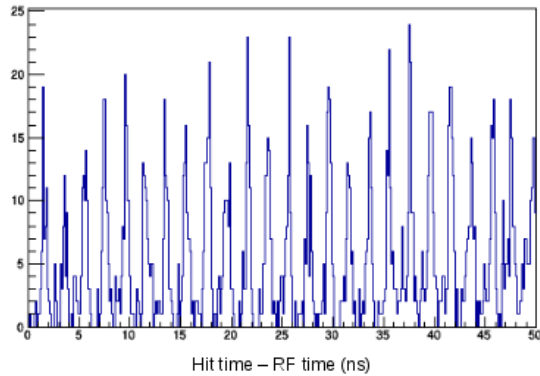

Figure 7: Difference in time between a single crystal hit and the RF time.

To evaluate m of eq 2, the time difference between clusters from Møellers and trident production is used. Correlated cluster candidates must have an energy sum close to the beam energy, an energy difference less than 200 MeV and occur in the same 40 ns time window. For each cluster, only the crystal with the highest energy is considered (seed hit) and the time difference between the two crystals recorded for each crystal. This procedure is repeated for each event. The resultant distributions provide again a 2 ns interval patern as seen in Figure 8 but this time the largest peak indicates the correct offset, thus the parameter m.
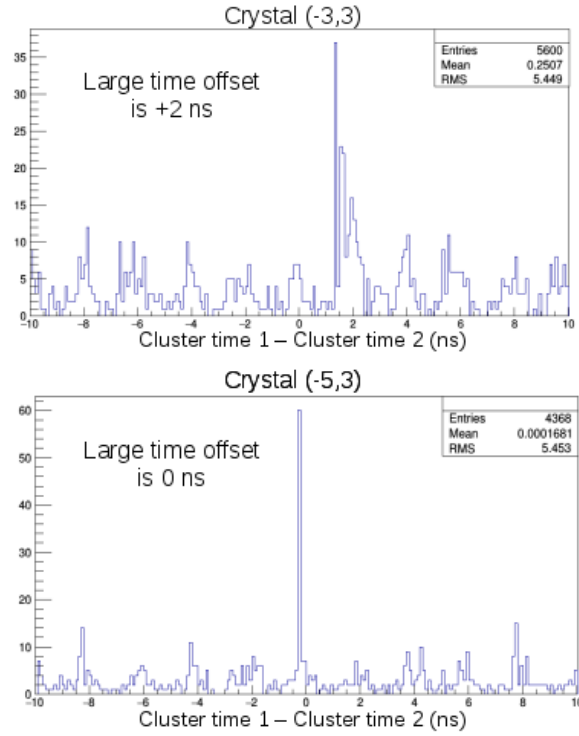

Figure 8: Time difference between the seed hit of two correlated clusters after RF calibration. The top and bottom plots show events for two different seed hit crystals.

The total time offset for each crystal can finally be obtained as the sum of the two methods and are presented in Figure 9). We notice that a particular

group has -4 ns time offsets, it corresponds to a group of channels using a shorter readout cable from the ECal to the FADC.
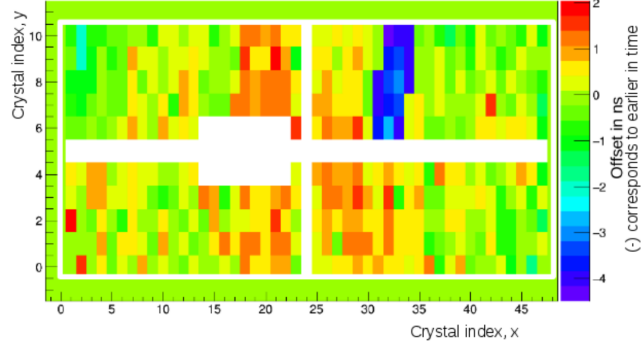

Figure 9: Individual time offsets for each crystal.

3.2. Energy dependent time walk

The time offsets can be energy dependent if there is time walk, we studied the difference of time between hits in a single cluster versus the highest energy hit as a function of energy. The results are fitted by an decreasing exponential and a second order polynomial, as shown in Figure 10, and be corrected.
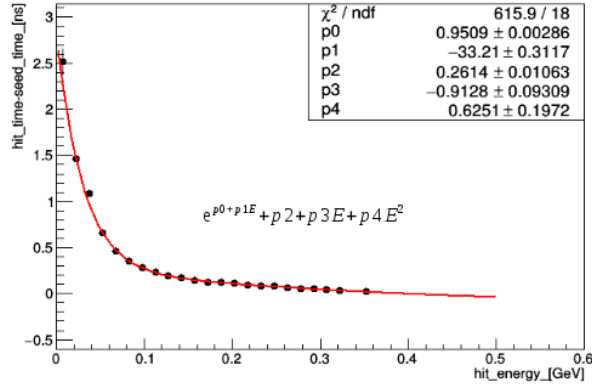

Figure 10: Time walk correction for clusters where the seed hit energy is greater than 400 MeV.

Finally, the time resolution as a function of the energy can be plotted from

11

the width of the time cluster time coincidences shown in Figure 11. We find this time resolution to be:

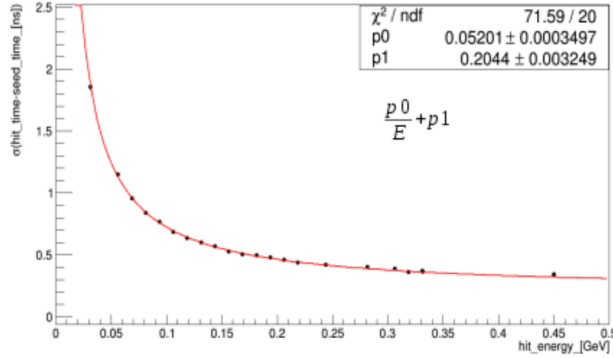$$\text{Time resolution} = \frac{0.052}{E \ (\text{GeV})} + 0.2044 \ \text{ns}. \tag{3}$$

Figure 11: Individual crystal time resolution as a function of energy.

The time resolution obtained shows the good performances of HPS electromagnetic calorimeter and a good capability to recover a time precision well below the initial sampling size (i.e. 4 ns).

4. Energy calibration

(Holly)

We should probably wait for the results with the new ECal geometry implementation. But, almost everything can be written and the plots will be added at the last moment.

Describe the method used to determine the energy calibrations: cosmics short description of the clustering algorithm: seed+crystals around+what we do with piled up clusters. Description of the events used for the calibration. Then results obtained with the method. Energy resolution as a function of the energy and position.

12

5. Trigger performance?

6. LED system

(Andrea)

We present here, the performances of the LED system.

7. Conclusions

Main points: - Good time resolution with large sampling - Importance (or not?) of crystal spacing for energy resolution ??? - Stability of the LED system

References